JOURNAL OF MATERIALS SCIENCE 10 (1975) 2016–2024

Equilibrium penny-like cracks in indentation fracture

B. R. LAWN*, E. R. FULLER
Institute for Materials Research, National Bureau of Standards, Washington, DC, USA

A study is made of the mechanics of two basic types of indentation fracture, cone cracks ("blunt" indenters) and median cracks ("sharp" indenters). The common feature which forms the central theme in this work is that both crack types, in their well-developed stages of growth, may be regarded as essentially "penny-like". On this basis a universal similarity relation is derived for equilibrium crack dimension as a function of indentation load. Experimental measurements confirm the general form of this relation. A more detailed fracture mechanics analysis is then given, to account for additional, contact variables evident in the data. Notwithstanding certain analytical limitations, the study serves as a useful basis for investigating a wide range of contact-related problems, both fundamental and applied, in brittle solids.

1. Introduction

Considerable interest has recently been shown in the crack patterns produced during the indentation of brittle surfaces. Apart from providing a novel means for measuring important fracture parameters (e.g. fracture surface energies, crack velocities), the individual indentation fracture event serves as a convenient "basic microscopic unit" in the ultimate description of a wide range of ceramics engineering properties (degradation, abrasion, wear, erosion, etc.) [1]. By far the greatest attention has been directed to the relatively well-defined crack configuration generated by a spherical indenter, the so-called Hertzian cone fracture [2, 3]. The sphere typifies "blunt" indenters, in which the contact prior to fracture remains predominantly elastic. By contrast, the more complex fracture patterns produced by "sharp" indenters (e.g. cone, pyramid) [4], where limited irreversible flow about the indenter point occurs as a necessary precursor to crack growth, have gone largely unstudied. Yet of the two extremes in indenter geometry, it is the sharp indenter which emerges as more pertinent in real contact situations where severity of surface damage is a prime concern [5, 6].

In this study we seek to establish a wider descriptive basis for the cracking that occurs in the general indentation of brittle solids, with particular emphasis on sharp indenters. For this purpose it becomes convenient to identify various phases in the evolution of the indentation fracture event, from crack initiation in the contact field to full-scale propagation in the advanced loading (and even unloading) stages. While somewhat arbitrary, this approach usefully highlights the similarities and differences in the blunt and sharp indenter patterns, and permits an adequate description of certain facets of a given fracture situation in cases where the overall behaviour appears hopelessly complex. It is found that the greatest differences occur in the earliest stages of indentation, the very mode of crack initiation depending critically on the geometrical distribution of contact stresses. Conversely, the similarities become more apparent in the well-developed stages, in which the far field of the applied loading now controlling crack growth is insensitive to details in the contact region. Ultimately, all well-developed indentation cracks tend to expand on an ever-increasing, near-circular front at advanced loading, thus assuming a penny-like configuration. It is this last aspect which forms the focal point in the present work.

*Present address: School of Physics, University of New South Wales, Kensington, N.S.W. 2033, Australia.

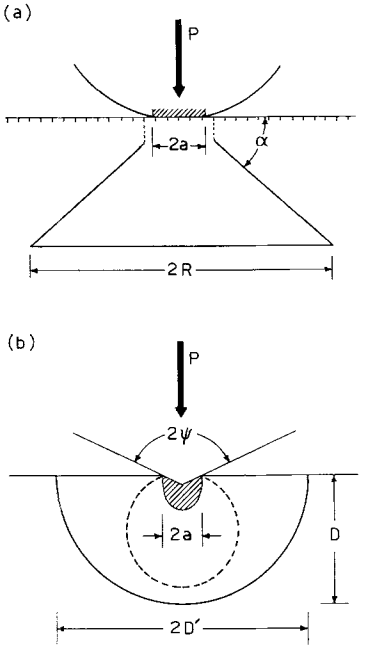

Figure 1 Basic indentation fracture systems. (a) Cone crack system, associated with "blunt" indenter: the crack nucleates from a pre-existing surface flaw (small dashes) outside contact (shaded), forms into a surface ring (broken line), and finally becomes critical and propagates into a fully developed cone. (b) Median crack system, associated with "sharp" indenter: the crack nucleates from plastic contact zone (shaded), forms into a contained penny (broken circle) and ultimately develops into a full half-penny.

2. General features of indentation fracture patterns

Fig. 1 illustrates the essential features of crack geometry for both blunt and sharp indenters, along with the relevant fracture mechanics parameters. In each case the indenter sets up a contact stress field, the tensile component of which provides the driving force for the ensuing fracture. If the applied load P were to be effectively concentrated at a point in the specimen surface (i.e. $a \rightarrow 0$), the intensity of the stresses would vary according to a simple inverse-square relation (the so-called Boussinesq field) [1, 4]. However, in reality the stress level cuts off at some finite limit within the contact region: with blunt indenters the cut-off is merely a manifestation of a redistribution in load over a nonzero, elastic contact area, whereas with sharp indenters it is associated more closely with the inability of the solid to sustain stresses greater than some "yield" value [4]. One may accordingly view the real distribution of stresses along the prospective crack path in terms of a hypothetical superposition of Boussinesq stresses and localised, near-contact "closure" stresses.*

In this context we investigate the evolution of the two situations depicted in Fig. 1, in the following sections.

2.1. Blunt indenters

2.1.1. Crack nucleation

Outside the elastic contact circle (whose radius is determined by the load, indenter size, and elastic constants) the stresses in a shallow "skin" layer, where surface flaws pre-exist, are highly tensile [2, 3, 8]. As the stress intensity builds up with increasing load, one or more of the flaws nucleates a crack.

2.1.2. Crack formation

The "dominant" flaw runs around the contact circle to form a shallow surface ring crack. Owing to the restraining action of the "closure" stresses, the newly formed ring does not, in general, extend spontaneously downward: the system must first overcome an energy barrier. Accordingly, the ring crack may be driven downward, either stably by purely mechanical forces (i.e. by increasing the indenter load) [2] or subcritically by combined mechanical and chemical forces (e.g. by introducing a reactive environment into the system) [9], until some critical depth (typically $\approx 0.1a$) is attained.

2.1.3. Crack propagation

Once beyond the critical, formation depth the surface ring propagates unstably into the full Hertzian cone, at a depth $\approx a$. The crack is then said to be "well-developed", in that details in the near-contact stress distribution no longer greatly influence the fracture mechanics. Increasing the driving force still further simply causes the cone to continue its propagation, in a stable manner.

2.1.4. Crack unloading

Upon unloading the system the cone crack tends to close (but rarely to heal) [10]. In certain contact situations frictional tractions between indenter and specimen may actually enhance growth of the cone system [11].

* The procedure is strongly analogous to that used in fracture theory to represent the complex non-linear stress field at the tip of a propagating crack [7].

2.2. Sharp indenters

2.2.1. Crack nucleation

In this case the contact is partially plastic, necessarily so because of a singularity about the sharp indenter point in an otherwise linear elastic field [4]. The plasticity somewhat relieves the tension locally about the contact area (whose dimension is now determined by the load, indenter shape, and material hardness). Instead, the greatest concentration of tensile stress occurs directly below the indenter point, and the crack nuclei are created there by the deformation process itself.

2.2.2. Crack formation

The deformation-induced crack nuclei grow as near-pennies, wholly contained beneath the contact zone, on median planes (planes containing the normal load axis) [4]. As with the Hertzian surface ring fractures, these so-called median cracks grow stably, but are susceptible to environmental effects. Depending on the indenter geometry, this formation stage may continue to a depth $\approx a$ or more. Several, mutually intersecting median cracks may form during the course of indentation.

2.2.3. Crack propagation

At some stage in the growth the median cracks begin to "break through" to the specimen surface; the restraining, compressive "hoop" stresses outside the contact area can no longer contain the expanding pennies [4]. This critical stage is not as well defined as the corresponding cone development in the Hertzian test, and the different coexisting median cracks may "pop-in" successively as the loading proceeds. The cracks then tend to the well-developed configuration of more or less symmetrical, stably propagating half-pennies centred on the contact point.

2.2.4. Crack unloading

Unloading the system causes the median cracks to close. However, with sharp indenters there are additional, residual-stress effects, attributable to incompatibility between the plastic zone and surrounding elastic material [12]; the mechanical mismatch appears to set up a "reversed field" just prior to complete withdrawal of the indenter. Thus the stresses which, on loading, acted to open up the median cracks, tend now to compression, thereby enhancing closure beneath the indenter. In the near-surface region, on the other hand, the reversal is of opposite sign, the development of a hoop tension actually opening up any partially contained penny cracks to the specimen surface.

The net result is, therefore, always a crack configuration close to the ideal half-penny shape, regardless of whether the fully propagating stage was reached during loading or not. A secondary manifestation of the residual stess field is the initiation of an entirely different, laterally extending system of cracks (not shown in Fig. 1b); these lateral cracks emanate from the deformation zone and grow in a saucer-shaped configuration toward the specimen surface, corresponding to a "chipping mode" of fracture [12].

3. Similarity relations for the penny-like cracks

In the interest of simplicity we proceed to an analysis of the indentation fracture problem on the assumption that crack growth is determined predominantly by point-load, Boussinesq stresses. Such an assumption effectively restricts the applicability of any fracture mechanics solution to the fully-developed stages of crack propagation. The preceding formation stages of crack growth may then be seen as precursor stages, in which the near-contact field exerts an initial perturbing restraint on the evolution of the fracture pattern.

With this simplification the way is open to an analysis in terms of a scaling argument, in which mathematical formalism may be conveniently circumvented. Roesler [13] used this approach to obtain a solution for the cone crack configuration, and in the present section we merely generalize Roesler's treatment. The idea is to make use of the geometrical similarity of the well-developed cracks, in conjunction with the fundamental Griffith energy-balance condition for crack extension [14], to derive a relationship between the size of the cracks and the indenter load. In this way, noting that *all* well-developed indentation cracks are of the same geometrical form, i.e. penny-like (in the sense that they extend on a near-circular front), we may obtain a general expesssion for equilibrium growth.

In accordance with the Griffith condition, one seeks the configuration for which the rate of increase of total surface energy just balances the rate of decrease of total mechanical energy as the crack expands. Since the area of the crack surface must scale with the square of the characteristic crack dimension, c say, the total surface energy must be of the form

$$U_S \propto \Gamma c^2, \quad (1)$$

where Γ is the fracture surface energy. Again, we may note that the intensity of the indentation stress field will be determined by the point load divided by a characteristic area ($\propto P/c^2$), that the strain energy density will be given by the square of the stress divided by an elastic modulus ($\propto P^2/c^4E$, where E is Young's modulus), and that the volume of stressed material associated with the field of the crack will scale with the cube of the crack dimension ($\propto c^3$), such that the total mechanical energy may be written

$$U_M \propto P^2/Ec. \quad (2)$$

The energy-balance requirement, $dU_S/dc = -dU_M/dc$, then gives

$$P^2/c^3 = \text{const.}\Gamma E \quad (3)$$

for equilibrium cracks.

In the point-load approximation used here all details of the contact conditions are effectively "washed out". However, we should expect the indenter size or shape to have some influence in the fracture mechanics, for, as we have seen, the very nature of the crack pattern (i.e. whether cone or median) is determined to a large extent by the contact geometry. Before taking up this issue in depth we shall first examine pertinent experimental data in connection with the verification of Equation 3.

4. Experimental measurements of cone and median cracks

Observations have been made of the manner in which the size of both cone and median cracks depends on indenter load. All tests were conducted on soda-lime float glass, 12.7 mm thick, under conditions close to equilibrium (namely under conditions effectively excluding water vapour from the cracks [15]). The progress of the cracks was followed either photographically or by travelling microscope; inaccuracies in the measuring techniques were found to be insignificant in comparison to the scatter in results from crack to crack.† A considerably greater proportion of the experimental effort was devoted to the median cracks, these being relatively undocumented in the literature.

4.1. Cone cracks

The cone crack tests were conducted within an environmental chamber, with the force on the

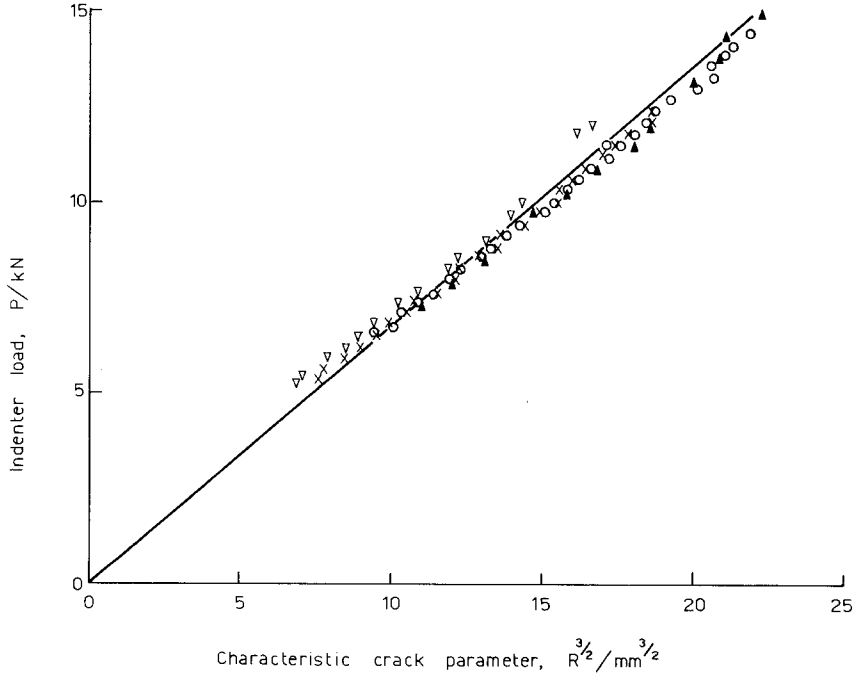

Figure 2 Results from observations of fully-developed cone crack in soda-lime glass. Data points from vacuum tests, using truncated spherical indenter. Each symbol represents a separate crack.

† As seen in the data of Figs. 2 to 5 below. Together with the data points, these figures include least-squares fits of Equation 3 (corresponding to a minimization of the error in $P/c^{3/2}$); the slopes of the lines thus fitted have a typical standard deviation of 5%.

indenter delivered by a dead-weight loading machine [16]. The indenter itself was a tungsten carbide sphere, but with a polished flat of 1 mm radius to maintain an invariant contact area (thus to ensure that the surface trace of the cone crack not be enveloped by an expanding contact circle). A light surface abrasion of the glass test slabs (e.g. in a slurry of No. 1000 SiC grit) prior to indentation served to introduce an abundance of suitable "pre-existing flaws" for crack initiation. The cracks were started by loading the specimens slowly, in moist air; this allowed for the controlled formation of well-defined surface rings, from which highly regular cones could be propagated. Having thus developed a crack, the chamber was evacuated ($\approx 10^{-4}$ Pa), and the base radius R of the stably propagating cone (representing the characteristic dimension c of Section 3) recorded as a function of increasing load P.

Fig. 2 shows the results, for four cracks. The plot is seen to be linear, within the scatter of the data. Equation 3 thus adequately represents the fracture mechanics for cone cracks.

4.2. Median cracks

For the median crack tests a standard Instron universal testing machine was used to deliver the indentation load. Indenters included six tungsten carbide cones ranging in half-angle from $\psi = 30°$ to 80° in 10° intervals, and a conventional Vickers diamond pyramid in a heavy-duty mount. The glass surfaces were indented in their as-received state. Initial loading was slow, to permit the median cracks to be formed in a controlled manner. For the sake of reasonable speed in the data accumulation, all subsequent crack propagation measurements were made in normal laboratory test environment.

The first set of such measurements involved following the depth D of the dominant median crack as a function of steadily increasing load P. In these tests the crosshair of a travelling microscope was continually translated to predetermined positions along the path of the expanding crack, and the load at the instant each crosshair position was reached by the crack tip appropriately recorded. This procedure conveniently provides the means for reducing the kinetic contribution to crack growth (due to the inevitable presence of water vapour) to a tolerably low level, through a simple adjustment of the Instron cross-head speed.

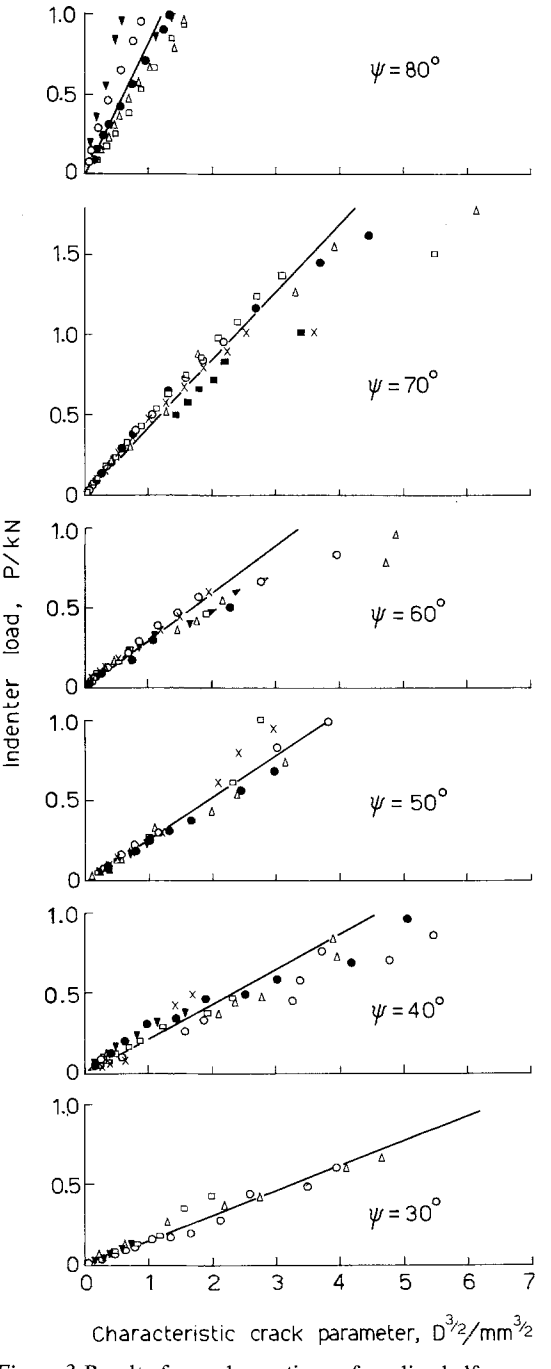

Figure 3 Results from observations of median half-penny cracks in soda-lime glass. Data points from tests in air, with the crack dimension recorded directly as a function of increasing load. Conical indenters, with half-angles as indicated. Each symbol represents a separate crack.

For instance, with a cross-head speed of 0.5 mm min^{-1} in the present experiments kinetic effects were estimated to give rise to increases of considerably less than 5% in the crack lengths.‡

‡ As adjudged from comparison with control tests in dry nitrogen atmosphere, in which slow crack growth effects were imperceptible.

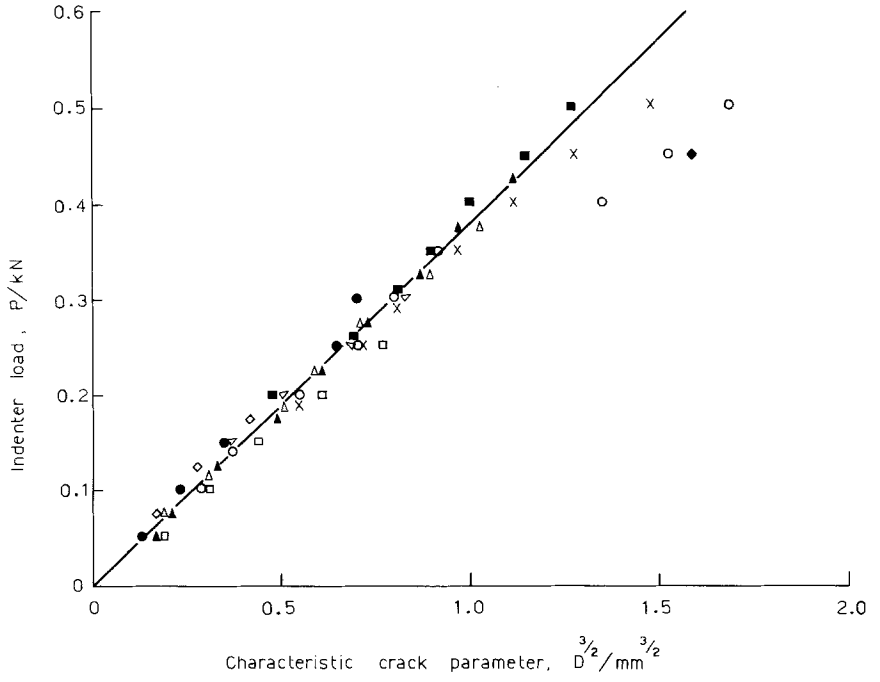

Figure 4 Results from observations of median half-penny cracks in soda-lime glass. Data points from tests in air, with the crack dimension recorded directly as a function of increasing load. Vickers pyramid indenter. Each symbol represents a separate crack. Compare the slope with those of Fig. 3 (the half-angle between opposing pyramid edges is 74°).

The data obtained are plotted in Figs. 3 and 4. As with the cone crack data, these plots confirm the essential form of Equation 3, within the limits of experimental reproducibility. However, certain additional features in the median crack results warrant further attention here. First, as a result of a greater variability in the crack pattern, the scatter in data becomes relatively pronounced at higher indentation loads. This trend could be directly associated with discontinuities in the downward growth of the leading median crack, corresponding to the sudden pop-in and expansion of intersecting neighbours. In general, the indentation process was typified by an extended sequence of abrupt load drops, these being most marked for the conical indenters of smaller half-angle. A second complicating feature was the tendency in the case of the most "blunt" conical indenter (i.e. $\psi = 80°$) for cone crack formation to precede median cracking. Here the plastic component of the contact is relatively small, and the effectiveness of pre-existing surface flaws as nucleation centres for fracture accordingly matches that of the deformation-induced flaws. The presence of the enveloping cone crack noticeably restricted the development of the contained median pennies.

A second set of measurements, prompted by the observation (Section 2.2) that any median cracks still in the formation stage tend to complete their development into the half-penny configuration during unloading, was taken from the residual crack patterns on the indented test surfaces. In these experiments the Instron cross-head velocity (0.5 mm min^{-1}) was simply reversed upon the attainment of some prescribed peak indentation load P'. The glass surfaces were then lightly etched in dilute hydrofluoric acid until the cracks were clearly visible, and the trace $2D'$ of the dominant median crack appropriately recorded for each indentation. Plots of the data thus obtained for conical indenters are given in Fig. 5, and may be compared with their analogues of Fig. 3.

5. More explicit fracture mechanics analysis

While the data of the previous section verifies the functional relationship between crack size and indenter load given in Equation 3, our fracture mechanics description remains incomplete. The emergence of contact geometry as an important factor in Figs. 2 to 5 emphasizes a major inadequacy in our simplistic treatment of Section 3. To account for this additional factor a more detailed analysis is necessary. We adopt the conventional fracture mechanics approach here, seeking

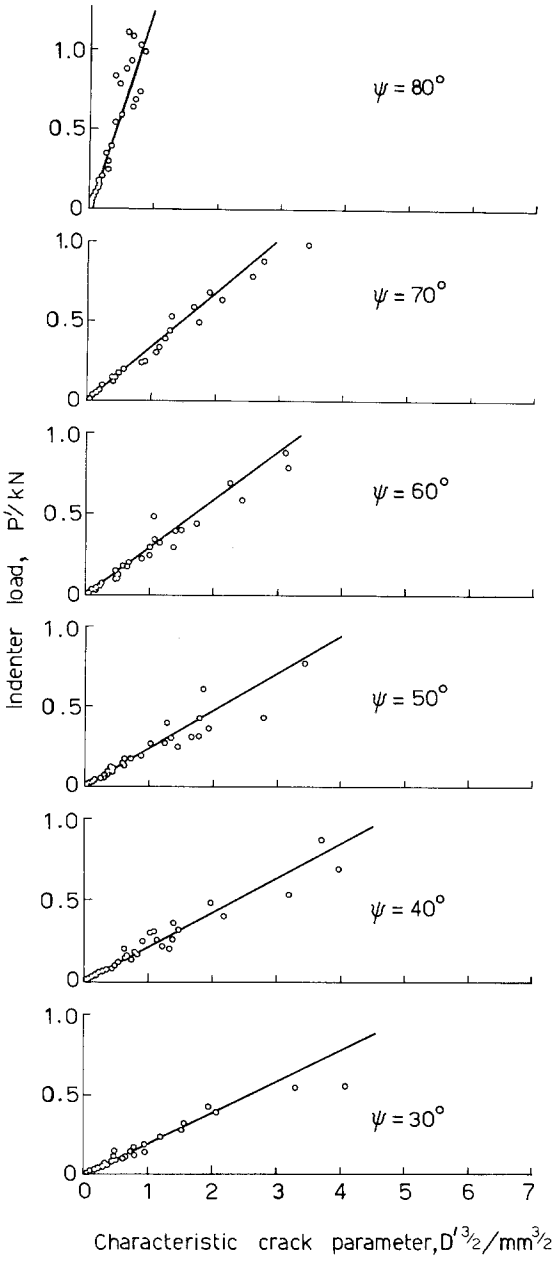

Figure 5 Results from observations of median half-penny cracks in soda-lime glass. Data points from tests in air, with the crack dimension recorded from residual surface trace as function of peak load. Conical indenters, with half-angles as indicated.

solutions for the crack-extension force G or stress-intensity factor K, from which equilibrium equations may once again be obtained via the Griffith condition, expressible as $G = K^2(1-\nu^2)/E$ (plane strain) [17].

5.1. Cone cracks

The case of well-developed cone cracks has already been treated rigourously in the paper by Roesler [13], and we shall do no more than quote Roesler's solutions. The crack-extension force, per unit width of crack front, is calculated as

$$G = \kappa_R^{\mathrm{p}}(\nu) P^2/ER^3 \tag{4}$$

where κ_R^{p} is a dimensionless constant uniquely determined by Poisson's ratio ν: the superscript p denotes a fully propagating crack and the subscript R identifies the characteristic crack dimension. In conjunction with the Griffith condtion, Equation 4 gives the equilibrium expression

$$P^2/R^3 = 2\Gamma E/\kappa_R^{\mathrm{p}}(\nu). \tag{5}$$

The dimensionless constant, although independent of the geometry of the indenter (provided the contact remains blunt), directly involves the cone crack angle α (Fig. 1a) according to [13]

$$\kappa_R^{\mathrm{p}}(\nu) = f(\nu)\,[\cos\alpha]_\nu. \tag{6}$$

This result, therefore, represents only a minor elaboration on the similarity relation, Equation 3. A numerical analysis by Roesler for $\nu = 0.25$ ($\alpha = 22°$) gives $\kappa_R^{\mathrm{p}} = 2.75 \times 10^{-3}$, whereas from the slope of Fig. 2 we obtain for soda-lime glass, using $\Gamma = 3.9\,\mathrm{J\,m^{-2}}$ and $E = 7.0 \times 10^{10}\,\mathrm{Pa}$ [18], the value $\kappa_R^{\mathrm{p}} = (1.19 \pm 0.10) \times 10^{-3}$.

5.2. Median cracks

For the median cracks we consider the centre-loaded half-penny configuration of Fig. 1b. We envisage a single well-developed crack driven primarily by the wedging component of indentation force, $P_\perp$, normal to the median plane. In the case of a smooth contact the wedging force is readily resolved in terms of the characteristic half-angle ψ of the indenter,

$$P_\perp = P/2 \tan\psi. \tag{7a}$$

More generally, for a rough contact, Equation 7a modifies slightly to

$$P_\perp = P/2 \tan\psi', \tag{7b}$$

with

$$\psi' = \psi \pm \arctan\mu, \tag{8}$$

μ being the coefficient of sliding friction; the plus sign in Equation 8 refers to the loading half-cycle, the minus sign to the unloading half-cycle. Contact friction may thus be regarded as either "blunting" (loading) or "sharpening" (unloading) the indenter.

The stress-intensity factor for the crack system

under consideration is obtainable from fracture mechanics handbooks [19],

$$K = 2P_{\perp}/(\pi D)^{3/2}. \quad (9)$$

(This equation omits a small correction factor associated with free-surface effects.) Incorporating Equations 7b and 9 into the Griffith condition, we have

$$P^2/D^3 = 2\Gamma E/\kappa_D^p(\nu, \psi') \quad (10)$$

in analogy to Equation 5, with the dimensionless constant

$$\kappa_D^p(\nu, \psi') = (1-\nu^2)/\pi^3 \tan^2 \psi'. \quad (11)$$

The geometrical term ψ', unlike its counterpart α in the cone crack system, varies independently of ν. Using the values of ν, Γ and E already specified, we may evaluate $\kappa_D^p(\psi)$ for soda-lime glass from the slopes of Figs. 3 and 5, and thence investigate the validity of the present analysis by plotting arctan $\{[(1-\nu^2)/\pi^3\kappa_D^p]^{1/2}\}$ as a function of ψ. According to Equations 11 and 8, such a plot should have a slope of unity and an intercept on the ordinate dependent on μ. However, the results of the present experiments, Fig. 6, are too uncertain to warrant an appropriate curve-fitting exercise; we recall in particular from Section 4.2 the tendency for the crack pattern to depart markedly from the ideal, single half-penny configuration at extremes in half-angle ψ. Instead, we simply plot the zero friction curve in Fig. 6 for comparison with the data.

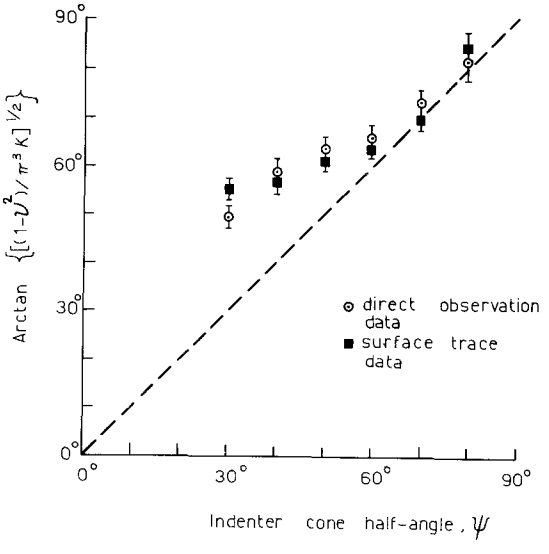

Figure 6 Plot of median crack data to investigate the validity of Equation 11.

6. Discussion

Our treatment of the indentation fracture problem derives from the rationalization that the well-developed cracks are basically penny-like in form. This is tantamount to assuming that the fracture mechanics are predetermined by a point-loading, Boussinesq-type stress field, in which case we should recognize certain limitations of the approach. For a start, as mentioned in Section 2, near-contact "closure" stresses operate to retard crack growth in the "formation" stage. The nature of these near-contact stresses determines, among other things, the "critical load" at which growth proceeds to the fully-developed stage [2, 4]. Thus, in using the present analysis to model ceramics engineering problems, we are restricted to the more severe indentation damage situations. A second limitation concerns the fact that the Boussinesq picture appears to be inadequate for describing the lateral cracks which form upon unloading sharp indenters (Section 2.2). Although its saucer-like geometry does preserve the most essential feature of the penny configuration (namely the outward expansion on a near-circular front), the lateral crack system evolves in an ill-defined residual stress field whose very source is not well understood [12]. This secondary crack type warrants further attention, for it relates closely to surface removal processes in brittle materials [1, 20].

At the same time, our circumvention of detailed descriptions of the near-contact stresses in the loading half-cycle, and of the residual stresses in the unloading half-cycle, has not been entirely restrictive. We have still been able to identify some parameters associated with the nature of the contact, such as α in Equation 6 for cone cracks and ψ and μ in Equations 8 and 11 for median cracks, although the role of these parameters could not be unequivocally established in the present experiments. Again, due recognition has been given to the important function of residual stresses in expanding partially contained median penny cracks to the specimen surface, thereby permitting one to infer the relevant fracture mechanics from examinations of crack traces on test surfaces after indentation [21]; the potential application of this correlation as a means for diagnosing the history of indentation damage events in brittle materials, especially in opaque materials, becomes obvious.

Indentation fracture presents itself as a useful

addition to the mechanical testing repertoire of the materials scientist [1]. Where the measurement of basic fracture mechanics parameters is the objective the theory given here should serve as an adequate framework for analysing the data, provided the indentation conditions are chosen such that a single, well-defined penny crack is produced: the cone crack system appears to be best suited for this purpose. Although we have considered only equilibrium cracks, an extension of the analysis to include kinetic effects is not impracticable: indeed, cone crack tests have actually been used to obtain crack velocity data on glass in moist environments [22]. Where an analysis of more practical contact damage situations is required one needs to bear in mind that the calculations are likely to overestimate the crack dimensions. This constitutes no real disadvantage in strength degradation studies, from which we emerge with a sound basis for conservative engineering design [5, 6]. Moreover, the distinction between blunt and sharp indenters, representing extremes in contact severity, provides convenient bounds for the description of real contact situations.

Acknowledgements

The authors are indebted to S. M. Wiederhorn and A. G. Evans for valuable discussions throughout this work. Sponsorship by the Office of Naval Research under Contract No. NR-032-535 is acknowledged.

References

1. B. R. LAWN and T. R. WILSHAW, *J. Mater. Sci.* **10** (1975) 1049.
2. F. C. FRANK and B. R. LAWN, *Proc. Roy. Soc. Lond.* **A299** (1967) 291.
3. T. R. WILSHAW, *J. Phys. D: Appl. Phys.* **4** (1971) 1567.
4. B. R. LAWN and M. V. SWAIN, *J. Mater. Sci.* **10** (1975) 113.
5. B. R. LAWN, S. M. WIEDERHORN and H. H. JOHNSON, *J. Amer. Ceram. Soc.*, in press.
6. B. R. LAWN, E. R. FULLER and S. M. WIEDERHORN, *ibid,* in press.
7. B. R. LAWN and T. R. WILSHAW, "Fracture of Brittle Solids" (Cambridge University Press, Cambridge, 1975) Ch. 4.
8. B. R. LAWN, *J. Appl. Phys.* **39** (1968) 4828.
9. A. G. MIKOSZA and B. R. LAWN, *ibid* **42** (1971) 5540.
10. J. S. WILLIAMS, B. R. LAWN and M. V. SWAIN, *Phys. Stat. Sol. (a)* **2** (1970) 7.
11. K. L. JOHNSON, J. J. O'CONNOR and A. C. WOODWARD, *Proc. Roy. Soc. Lond.* **A334** (1973) 95.
12. B. R. LAWN, M. V. SWAIN and K. PHILLIPS, *J. Mater. Sci.* **10** (1975) 1236.
13. F. C. ROESLER, *Proc. Phys. Soc.* **B69** (1956) 981.
14. A. A. GRIFFITH, *Phil. Trans. Roy. Soc. Lond.* **A221** (1920) 163.
15. S. M. WIEDERHORN, *J. Amer. Ceram. Soc.* **50** (1967) 407.
16. J. J. H. BEEK and B. R. LAWN, *J. Phys. E: Sci. Instrum.* **5** (1972) 710.
17. In [7], Ch. 3.
18. S. M. WIEDERHORN, *J. Amer. Ceram. Soc.* **52** (1969) 99.
19. P. C. PARIS, and G. C. SIH, *Amer. Soc. Test. Mater., Spec. Tech. Publ.* **381** (1965) 30.
20. B. R. LAWN, *Wear* **33** (1975) 369.
21. J. R. VARNER and H. J. OEL, *Glastechn. Ber.*
22. M. V. SWAIN and B. R. LAWN, *Int. J. Fract.* **9** (1973) 481.

Received 23 May and accepted 27 May 1975.